PCCP

ROYAL SOCIETY OF CHEMISTRY

PAPER

View Article Online
View Journal | View Issue

Check for updates

Cite this: *Phys. Chem. Chem. Phys.*, 2023, **25**, 15855

Exploring mechanochemical reactions at the nanoscale: theory *versus* experiment†

Nicholas Hopper,[a] François Sidoroff,[b] Resham Rana,[a] Robert Bavisotto,[a] Juliette Cayer-Barrioz,[b] Denis Mazuyer[b] and Wilfred T. Tysoe*[a]

Mechanochemical reaction pathways are conventionally obtained from force-displaced stationary points on the potential energy surface of the reaction. This work tests a postulate that the steepest-descent pathway (SDP) from the transition state to reactants can be reasonably accurately used instead to investigate mechanochemical reaction kinetics. This method is much simpler because the SDP and the associated reactant and transition-state structures can be obtained relatively routinely. Experiment and theory are compared for the normal-stress-induced decomposition of methyl thiolate species on Cu(100). The mechanochemical reaction rate was calculated by compressing the initial- and transition-state structures by a stiff copper counter-slab to obtain the plots of energy *versus* slab displacement for both structures. The reaction rate was also measured experimentally under compression using a nanomechanochemical reactor comprising an atomic-force-microscopy (AFM) instrument tip compressing a methyl thiolate overlayer on Cu(100) (the same system for which the calculations were carried out). The rate was measured from the indent created on a defect-free region of the methyl thiolate overlayer, which also enabled the contact area to be measured. Knowing the force applied by the AFM tip yields the reaction rate as a function of the contact stress. The result agrees well with the theoretical prediction without the use of adjustable parameters. This confirms that the postulate is correct and will facilitate the calculation of the rates of more complex mechanochemical reactions. An advantage of this approach, in addition to the results agreeing with the experiment, is that it provides insights into the effects that control mechanochemical reactivity that will assist in the targeted design of new mechanochemical syntheses.

Received 2nd March 2023,
Accepted 17th May 2023

DOI: 10.1039/d3cp00980g

rsc.li/pccp

Published on 31 May 2023. Downloaded by University of Wisconsin-Milwaukee Libraries on 8/7/2023 6:46:01 PM.

Introduction

The rates of chemical reactions can be accelerated in several ways: by heating, by photons,[2] by electrons,[3] or by supplying mechanical energy in a field known as mechanochemistry. Despite mechanochemical reactions having been known for millennia[4] and having been studied by luminaries such as Michael Faraday,[5] the subfield of mechanochemistry remains less developed than the rest. However, over the past few years, a large number of active and selective organic and inorganic syntheses have been discovered by trial and error.[6,7] Methods that combine mechanochemical activation with catalysis have also achieved remarkable results such as the ability to synthesize ammonia from hydrogen and nitrogen at room temperature and modest pressures[8–11] to mimic the Haber–Bosch process that typically occurs at a pressure of 200 to 400 atmospheres and a temperature of ~500 °C.[12,13]

Single-molecule mechanochemical experiments were carried out by attaching the reacting system (known as a mechanophore) to an atomic force microscope (AFM) tip and by measuring the force needed to extend, and finally cleave, one or more bonds.[14–21] Because of the ability to accurately measure these forces, this approach can lead to precise measurements of force-induced bond scission rates. Many biological processes also involve forces exerted by or acting on molecular systems.[22–26]

One of the first theoretical approaches to analyzing the results of single-molecule experiments was the constrained geometries simulate external force (CoGEF)[27] method, which displaces the attachment (AP) and pulling points (PP) and then allows the perturbed system to relax to a new stable configuration to calculate the energy as a function of the force.[28–30] Analogous approaches include the force-modified potential energy surface (FMPES) method,[31,32] in which the PES is

[a] *Department of Chemistry and Biochemistry, University of Wisconsin-Milwaukee, Milwaukee, WI 53211, USA. E-mail: wtt@uwm.edu*
[b] *Laboratoire de Tribologie et Dynamique des Systèmes, CNRS UMR5513, Ecole Centrale de Lyon, F-69134 Ecully cedex, France*

† Electronic supplementary information (ESI) available: Calibration of normal stresses and reaction rates; atomic coordinates for the compression of methyl thiolate species on Cu(100); background subtraction methods for calculating the energy *versus* slab separation. See DOI: https://doi.org/10.1039/d3cp00980g

Published on 31 May 2023. Downloaded by University of Wisconsin-Milwaukee Libraries on 8/7/2023 6:46:01 PM.

modified by directly including the effect of the forces on the AP and PP. Mechanochemical reaction rates under hydrostatic pressure have been analyzed by the generalized force-modified potential energy surface (G-FMPES)[32–34] and the EFEI (external force is explicitly included) methods.[35]

Chemical reactions are analyzed in the framework of the Born–Oppenheimer potential-energy surface (BOPES). This complicated, multi-dimensional surface contains local energy minima due to atomic configurations that correspond to stable chemical compounds. The conversion between them constitutes chemical reactions and requires the transition over an energy barrier; otherwise, the reaction would occur spontaneously. The lowest-energy route between two metastable states (a reactant and product) passes over a saddle point, known as the transition state, *via* the so-called activated complex. This concept allows a complicated multidimensional problem to be reduced to a one-dimensional one. The quickest reaction path from the activated complex to the reactant is taken to be the steepest-descent pathway (SDP). The methods for calculating transition-state structures and the SPD are common and easy to implement.[36–40]

The general physical concepts that underpin mechanochemistry are based on the idea that the imposed force modifies the BOPES of the chemical reaction to change the energies and locations of the initial and transition states. This modifies the activation energy, thereby changing the reaction rate. Similar concepts also explain friction and viscosity.[41] The way in which the BOPES is modified by the force depends on its direction and magnitude. The reaction then follows the SDP on this modified BOPES along the so-called force-displaced stationary points (FSDPs).[42–45] However, calculating a FDSP for the chemical reaction requires knowing the shape of the BOPES, which can be tedious to compute. It has been recently proposed that mechanochemical reactions could be analyzed with good accuracy using the SDP and experimental evidence was presented to support this postulate.[46] Since the SDP is relatively easy to compute, this provides an efficient approach to calculating mechanochemical reaction rates. This idea is tested in this work.

An additional challenge for testing mechanochemical theories, in particular, for stress-induced reactions as opposed to those carried out by pulling single molecules, is to exert precise stresses on well-defined systems and to accurately measure their reaction rates. We address this issue by using a nano-mechanochemical reactor of about 60 nm^2 in size[47] formed by compressing a reactant-covered single-crystal substrate using an AFM tip.[41,48] This allows elastic contact mechanics to be used to calculate the stresses at the center of the contact[49] and to ensure that the reaction rate is measured on pristine regions of the surface.[1,47] We study the surface mechanochemical decomposition of methyl thiolate (CH_3–S) on Cu(100), where the mechanical reaction pathway has been extensively investigated under ultrahigh-vacuum conditions, which we have previously demonstrated can decompose under the influence of normal stresses.[1,50,51] This model system is sufficiently simple that it is amenable to analysis using first-principles density-functional theory (DFT) calculations. The results of calculations obtained using the SDP successfully reproduce the experimental results, confirming the validity of our initial postulate.

Background: the mechanochemical reaction pathway

The mechanochemical reaction pathway for methyl thiolate decomposition on clean Cu(100) has been extensively investigated in ultrahigh vacuum (UHV).[50,52–56] The methyl thiolate species is grafted to Cu(100) by exposure to dimethyl disulfide,[57] and is thermally stable up to ~450 K. Lateral shear and normal stresses accelerate the reaction rate by lowering the activation barrier from ~100 kJ mol^{-1} to a value that is low enough that the reaction proceeds at room temperature.[1,47] The calculated energy profile for methyl thiolate decomposition is shown in Fig. 1, where the activation energy is in good agreement with the experimental value obtained from temperature-programmed desorption (TPD) experiments.[51] The pathway from the transition state to the initial minimum (the methyl thiolate reactant) corresponds to the SDP. The insets show how the methyl thiolate structure evolves as the reaction proceeds. This is also shown as a movie in Fig. S1 (ESI†). This process occurs by the terminus of the methyl thiolate mechanophore moving both laterally and vertically with respect to the surface. Note that the reaction is still thermally driven and mechanochemical reaction rates depend on temperature. This predicts that both normal and lateral stresses should be effective in lowering the energy barrier; this work investigates the influence of normal stresses. Note that the evolution of the electronic structure during the course of a mechanochemical reaction is the same as for the thermal one.[14]

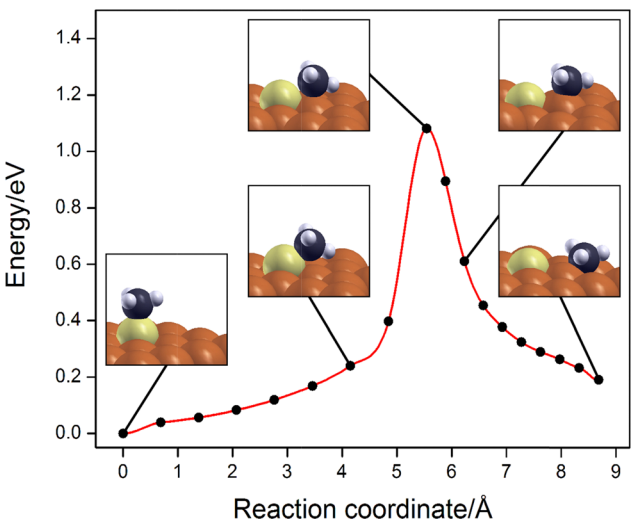

Fig. 1 Plot of the reaction profile for the decomposition of methyl thiolate species on a Cu(100) substrate[1] calculated using the density functional theory, where it reacts to form an adsorbed methyl species and adsorbed sulfur.

 This journal is © the Owner Societies 2023

Published on 31 May 2023. Downloaded by University of Wisconsin-Milwaukee Libraries on 8/7/2023 6:46:01 PM.

This work focusses just on normal-stress accelerated reactions, not those that are induced by a shear stress. The latter are more complicated because, unless the experiment is designed to impose a static shear, the rates will be velocity (as well as stress and temperature) dependent.[58–60]

Theoretical and experimental methods

Density functional theory (DFT) calculations of methyl thiolate overlayers on Cu(100) were performed by the projector augmented wave method[61,62] as implemented using the Vienna *Ab initio* Simulation Package (VASP).[63–65] The exchange–correlation potential was described using the generalized-gradient approximation of Perdew, Burke and Ernzerhof.[66] A cutoff of 400 eV was used for the planewave basis set, and the wavefunctions and electron density were converged to within 1×10^{-6} eV. The first Brillouin zone was sampled using a $4 \times 4 \times 1$ Monkhorst–Pack grid.[67] Geometric relaxations were considered to be converged when the force was less than 0.01 eV $Å^{-1}$ on all unrestricted atoms. van der Waals' interactions were implemented using the DFT-D3 method, as described by Grimme *et al.*[68] The reaction profile and the transition-state structure (as shown in Fig. 1) were calculated by the climbing nudged-elastic band (cNEB) method.[36,37,40]

Normal loads were exerted on the initial- and transition-state structures of methyl thiolate on a Cu(100) slab with a lattice constant of 3.575 Å, as shown in the movie in Fig. S2 (ESI†). The system consisted of two (2×2) Cu(100) slabs to mimic the experimentally measured saturation coverage of alkyl thiolates on Cu(100).[69] The initial- and the transition-state alkyl thiolate structures were adsorbed onto the bottom 6-layer slab. The bottom three layers of that slab were frozen, while the top three layers were allowed to relax. A counterface slab located above the adsorbate-covered substrate was used to exert a force on the thiolate overlayer to mimic the AFM compression experiment. The upper slab was three copper atomic layers thick and was passivated by hydrogen atoms located in the four-fold hollow sites of the slab to render the interacting surface chemically inert. All atoms in this slab were kept frozen to simulate an infinitely stiff surface. The initial coordinates of the system at a large initial separation are included in the ESI.† Compression of the methyl thiolate molecule was simulated by translating the hard slab in 0.1 Å steps along a direction perpendicular to the plane of the methyl-thiolate-covered slab. Decompression was simulated by raising the slab, also in 0.1 Å steps. Because the slabs were not identical, the surface charges induced by the different locations of the Fermi energies caused a long-range electrostatic interaction that resulted in approximately $1/d$ energy dependence, where d is the slab separation. The resulting energy *versus* distances curves are shown in Fig. S3 (ESI†) prior to the removal of the background, which was too large to be removed using the dipole–correction subroutine in the VASP software. Thus, the background was removed by carrying out separate single-point calculations of approaching slabs without an adsorbed methyl thiolate overlayer. The calculations also determined the strength of the interaction between the adsorbed methyl thiolate and the top slab. These interactions are discussed in greater detail in the ESI.† The sum of the interaction energies was subtracted from the approach curves with methyl thiolate present to lead to flat regions as the two slabs approached until they reached a repulsive region for which the energy increased approximately quadratically with the decreasing slab separation. These calculations were performed for both the reactant and transition-state structures.

The extent of reaction was measured from the depths of indents formed by pressing the AFM tip on the methyl-thiolate-saturated Cu(100) surface as a function of time, where the surface was imaged at a low, non-perturbative load.[1] Previous work has shown that similar methyl thiolate reaction pathways as discussed above are also induced by an AFM tip on a Cu(100) surface in UHV.[46] An example plot is shown in Fig. S8 (ESI†), which shows that the maximum depth is ~200 nm, similar to the height of a methyl thiolate species on copper. A fit to the data yields a first-order, stress-dependent rate constants, $k(\sigma)$, identical to the reaction order found for ball-on-flat sliding in UHV.[56] The normal stress was calculated from the diameter of the indent to gauge the contact area and the normal force exerted on the tip as described in the ESI.†

Results: normal-stress induced decomposition of methyl thiolates on Cu(100)

We tested the postulate that the reactant and transition-state structures connected by the SDP can be used to calculate the mechanochemical reaction rates. The resulting calculated energies of the compressed methyl thiolate reactant (■) and the transition-state (■) structures are plotted as a function of slab separation, as shown in Fig. 2, where the abscissa is shifted so that the origin coincides with the point of contact of the initial state (methyl thiolate) with the counterface. A video of the structural evolution is depicted in Fig. S2 (ESI†).

The energy difference at large separations is ~104 kJ mol^{-1}, in agreement with the calculated (Fig. 1) and the experimental reaction activation energies measured by TPD.[51] The energies stay constant until the rigid slab encounters the adsorbed species, where the methyl thiolate reactant contacts the counterface slab at larger separations than the geometrically lower transition-state structure at $x = 0.73 \pm 0.04$ Å. The applied normal force multiplied by this distance is the work done in going from the reactant to the activated complex and corresponds to an activation length, $\Delta x^{\ddagger}$.[48] This is conceptually analogous to the definition used in single-molecule pulling experiments, where it is the difference between the AP and PP in the initial and transition states.[26]

This leads to a formula for the force-dependent activation energy: $E_{act}(F_N) = E^0_{act} + \Delta x^{\ddagger} F_N$, where F_N is the normal force and E^0_{act} is the intrinsic activation energy. This is known as

Published on 31 May 2023. Downloaded by University of Wisconsin-Milwaukee Libraries on 8/7/2023 6:46:01 PM.

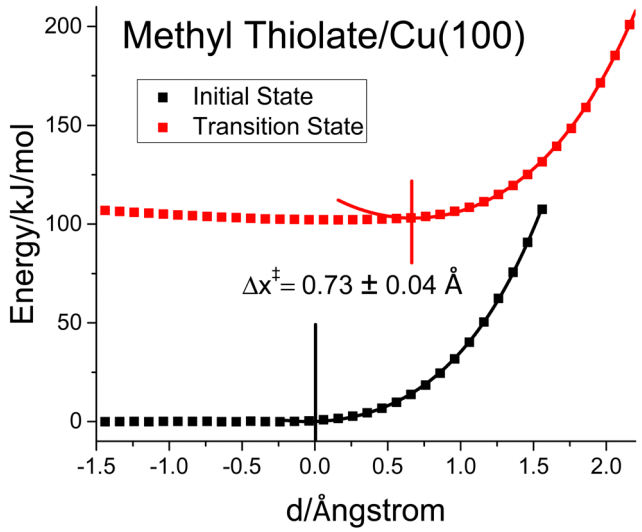

Fig. 2 Plot of the corrected energy *versus* slab separation for the initial (■) and transition (■) states for the normal-stress-induced decomposition of methyl thiolate on Cu(100). The slab separation axis has been moved, so that it is referenced to the minimum of the initial (reactant) state.

the Bell model.[70] Note that the value of $\Delta x^{\ddagger}$ depends on the direction of the force relative to reactant and transition-state structures.

The results in Fig. 2 indicate that these interactions are compliant and that the activation length itself depends on the force. Assuming that the distortion is harmonic as shown by the solid lines fitted to the theoretical results in Fig. 2, results in the so-called extended-Bell model:[48,71–73]

$$E_{act}(F_N) = E^0_{act} + \Delta x^{\ddagger} F_N + \frac{F_N^2}{2}(\chi_T - \chi_I) \qquad (1)$$

where χ_T (=1/k_T) and χ_I (=1/k_I) are the transition- and initial-state compliances and k_T and k_I are the corresponding force constants, where k_I = 16.8 ± 0.2 N m^{-1} and k_T = 25.8 ± 0.2 N m^{-1}. The average normal force exerted on each reactant, F_N, is calculated from the normal stress σ_{zz}, where the z axis is taken to be perpendicular to the surface, by $\sigma_{zz} = F_N/A_C$ where A_C is the area subtended by each methyl thiolate adsorbate over which the normal stress acts. Since $\Delta x^{\ddagger} F_N = \Delta x^{\ddagger} A_C \sigma_{zz}$, this yields a value of the activation volume $\Delta V^{\ddagger} = A_C \Delta x^{\ddagger}$, as first proposed by Stearn and Eyring.[74] A value of A_C = 26.12 Å^2 is calculated from the area occupied by a (2 × 2) methyl thiolate overlayer on Cu(100)[69] and leads to $\Delta V^{\ddagger} = \Delta x^{\ddagger} A_C = -19.1 \pm 1.0$ Å^3 molecule^{-1}. This indicates that the activation volume does not just depend on the nature of the reaction pathway, but also on the direction of the force relative to it. In this case, the activation volume comprises a cylinder of length ∼0.73 Å perpendicular to the surface with a cross-sectional area of ∼26 Å^2 parallel to it.

The form of eqn (1) is similar to those derived using the FDSP. However, the formula in eqn (1) is calculated from the data for the steepest-descent pathway. Eqn (1) can be written directly in terms of the normal stress, and σ_{zz} to mimic the experimental conditions using the Stearn–Eyring postulate to give:

$$E_{act}(\sigma_{zz}) = E^0_{act} + \Delta x^{\ddagger} A_C \sigma_{zz} + \frac{A_C^2 \sigma_{zz}^2}{2}(\chi_T + \chi_I)$$
$$= E^0_{act} + \Delta V^{\ddagger} \sigma_{zz} + \frac{A_C^2 \sigma_{zz}^2}{2}(\chi_T + \chi_I) \qquad (2)$$

Note that all the parameters required to evaluate eqn (2) are available from the plots in Fig. 2.

The results of these calculations are compared with the experimental data and a plot of ln k(σ) *versus* normal stress (■) is shown in Fig. 3,[1] which is an almost straight line with just a slight curvature. Note that stresses up to ∼1.6 GPa can routinely be obtained using the AFM nanoreactor and that this stress reduces the activation energy by ∼15 kJ mol^{-1} from the intrinsic value.[46]

To compare directly with experiment, eqn (2) is written as follows:

$$\ln(k(\sigma_{zz})) = \ln(k_0) - \frac{\Delta V^{\ddagger}}{k_B T}\sigma_{zz} - \frac{A_r^2 \sigma_{zz}^2}{2k_B T}(\chi_T + \chi_I) \qquad (3)$$

where k_0 is the zero-pressure rate constant, k_B is the Boltzmann constant and T is the absolute temperature. The value of k_0 (the value at zero stress) is obtained from the Arrhenius equation: $k_0 = A \exp\left(-\frac{E^0_{act}}{k_B T}\right)$, where A is a pre-exponential factor that is set to a value of 1 × 10^{13} s^{-1} that was used to calculate the activation energy from the peak temperature in TPD experiments for methyl thiolate decomposition on Cu(100).[51] Note that the lack of data between ∼0.6 GPa and this data point is due to the fact that mechanochemical reaction rates are too slow to be measured for lower stresses. The fact that the mechanochemically measured reaction rates extrapolate

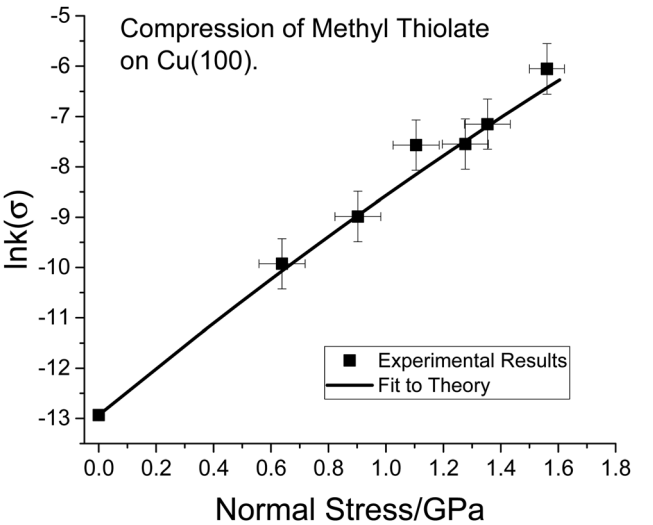

Fig. 3 Plot of the logarithm of rate of the normal-stress-induced decomposition of methyl thiolate decomposition on Cu(100) as a function of the normal stress in GPa (■)[1] compared with the theoretical plot from eqn (3) using parameters derived from the data in Fig. 2, so that the plot requires no adjustable parameters.

 This journal is © the Owner Societies 2023

Published on 31 May 2023. Downloaded by University of Wisconsin-Milwaukee Libraries on 8/7/2023 6:46:01 PM.

almost linearly to the rate at zero stress measured using a completely different method confirms that we are correctly measuring the mechanochemical kinetics for the same reactions.

The prediction from eqn (3) is also plotted in Fig. 3 and the agreement between the experimental data (■) and the theory (solid line) is very good.[56] It should be emphasized that the theoretical plot involves no adjustable parameters and uses only values obtained from Fig. 2, a value of the pre-exponential factor (A) to relate the activation energy to the rate constant, and the value of A_C used in the Stearn–Eyring postulate. Note that the activation volume here is larger than previously reported[1] because of refinements in the calibration of the contact areas and forces as described in the ESI.†

The good agreement between experiment and theory over a relatively wide stress range confirms that (i) the SDP can be used with good accuracy to calculate the mechanochemical reaction rates and (ii) the Stearn–Eyring postulate can be used to calculate the activation volume. The results show that, at least in this case, a linear force dependence reproduces the experimental results quite well and obeys the Bell model, suggesting that the F^2 contributions are small, although a slight curvature is noticeable in the data in Fig. 3.

It also emphasizes that both the value of the activation length and the area over which the stresses act can influence the activation volume. The latter parameter can be controlled by modifying the structure of the mechanophore in a targeted way to modulate the force exerted along the SDP. The results also illustrate how the direction of the stress relative to the structure of the mechanophore influences the mechanochemical reactivity and can induce reactions that are not thermally accessible.[75]

Conclusions

This work tested the postulate that mechanochemical reaction rates can be calculated by the steepest-decent pathway[46] using the example of the normal-stress-induced decomposition of methyl thiolate on Cu(100). The reaction rate was measured using a nanomechanochemical reactor that allows the contact stresses and the reaction rates to be measured.

The calculation was carried out by compressing the initial- and transition-state structures by a rigid counterface to provide values of the activation length and the compliances of the initial- and transition-states for use as parameters in an extended-Bell model. The activation volume was calculated from the product of the activation length, and the area over which the force acts as first suggested by Stearn and Eyring. The results agreed very well with the experiment confirming the postulate that using the SDP as the mechanochemical reaction pathway provides a good approximation that yields stress-dependent energies that are in good agreement with those measured experimentally. The advantages of this approach are that the calculations are easy to perform and the obtained results are in good agreement with experiment. This, of course, needs to be tested for other more complex mechanochemical reactions.

Author contributions

All authors contributed equally to the paper.

Conflicts of interest

There are no conflicts to declare.

Acknowledgements

We gratefully acknowledge the Civil, Mechanical and Manufacturing Innovation (CMMI) Division of the National Science Foundation under grant number 2020525 for support of this work. This work was also supported by the French Agency for Ecological Transition (ADEME) through the IMOTEP project. We also thank Professor Filippo Mangolini for very useful discussions.

References

1 A. Boscoboinik, D. Olson, H. Adams, N. Hopper and W. T. Tysoe, *Chem. Commun.*, 2020, **56**, 7730–7733.
2 D. C. S. Bryce-Smith, *Photochemistry, Chemical Society*, London, England, 1970.
3 J. O. M. Bockris, *Electrochemistry, Butterworths*, University Park Press, London; Baltimore, 1973.
4 H. J. Theophrastus, *Theophrastus's history of stones: with an English version, and critical and philosophical notes, including the modern history of the gems, &c., described by that author, and of many other of the native fossils*, London, 1774.
5 M. M. J. K. Faraday, *Chemical manipulation: being instructions to students in chemistry on the methods of performing experiments of demonstration or of research with accuracy and success*, Carey and Lea, Philadelphia, 1831.
6 S. L. James, C. J. Adams, C. Bolm, D. Braga, P. Collier, T. Friscic, F. Grepioni, K. D. M. Harris, G. Hyett, W. Jones, A. Krebs, J. Mack, L. Maini, A. G. Orpen, I. P. Parkin, W. C. Shearouse, J. W. Steed and D. C. Waddell, *Chem. Soc. Rev.*, 2012, **41**, 413–447.
7 J.-L. Do and T. Friščić, *ACS Cent. Sci.*, 2017, **3**, 13–19.
8 F. Haber and R. Le Rossignol, *Z. Elektrochem. Angew. Phys. Chem.*, 1913, **19**, 53–72.
9 G. Ertl, *Catal. Rev.*, 1980, **21**, 201–223.
10 N. D. Spencer, R. C. Schoonmaker and G. A. Somorjai, *Nature*, 1981, **294**, 643–644.
11 N. D. Spencer, R. C. Schoonmaker and G. A. Somorjai, *J. Catal.*, 1982, **74**, 129–135.
12 G.-F. Han, F. Li, Z.-W. Chen, C. Coppex, S.-J. Kim, H.-J. Noh, Z. Fu, Y. Lu, C. V. Singh, S. Siahrostami, Q. Jiang and J.-B. Baek, *Nat. Nanotechnol.*, 2021, **16**, 325–330.
13 S. Reichle, M. Felderhoff and F. Schüth, *Angew. Chem., Int. Ed.*, 2021, **60**, 26385–26389.

Published on 31 May 2023. Downloaded by University of Wisconsin-Milwaukee Libraries on 8/7/2023 6:46:01 PM.

14 J. J. Gilman, *Science*, 1996, **274**, 65.
15 F. K. Urakaev and V. V. Boldyrev, *Powder Technol.*, 2000, **107**, 93–107.
16 F. K. Urakaev and V. V. Boldyrev, *Powder Technol.*, 2000, **107**, 197–206.
17 M. K. Beyer and H. Clausen-Schaumann, *Chem. Rev.*, 2005, **105**, 2921–2948.
18 D. A. Davis, A. Hamilton, J. Yang, L. D. Cremar, D. Van Gough, S. L. Potisek, M. T. Ong, P. V. Braun, T. J. Martínez, S. R. White, J. S. Moore and N. R. Sottos, *Nature*, 2009, **459**, 68–72.
19 H. M. Klukovich, T. B. Kouznetsova, Z. S. Kean, J. M. Lenhardt and S. L. Craig, *Nat. Chem.*, 2013, **5**, 110–114.
20 J. R. Felts, A. J. Oyer, S. C. Hernández, K. E. Whitener Jr, J. T. Robinson, S. G. Walton and P. E. Sheehan, *Nat. Commun.*, 2015, **6**, 6467.
21 P. Seema, J. Behler and D. Marx, *Phys. Chem. Chem. Phys.*, 2013, **15**, 16001–16011.
22 H. Khataee and A. Wee-Chung Liew, *Bioinformatics*, 2013, **30**, 353–359.
23 K. Sasaki, M. Kaya and H. Higuchi, *Biophys. J.*, 2018, **115**, 1981–1992.
24 J. Zlatanova, S. M. Lindsay and S. H. Leuba, *Prog. Biophys. Mol. Biol.*, 2000, **74**, 37–61.
25 C. Zhu and R. P. McEver, *Mol. Cell. Biomech.*, 2005, **2**, 91–104.
26 D. E. Makarov, *J. Chem. Phys.*, 2016, **144**, 030901.
27 M. K. Beyer, *J. Chem. Phys.*, 2000, **112**, 7307–7312.
28 Z. Huang and R. Boulatov, *Chem. Soc. Rev.*, 2011, **40**, 2359–2384.
29 T. J. Kucharski and R. Boulatov, *J. Mater. Chem.*, 2011, **21**, 8237–8255.
30 I. M. Klein, C. C. Husic, D. P. Kovács, N. J. Choquette and M. J. Robb, *J. Am. Chem. Soc.*, 2020, **142**, 16364–16381.
31 M. T. Ong, J. Leiding, H. Tao, A. M. Virshup and T. J. Martínez, *J. Am. Chem. Soc.*, 2009, **131**, 6377–6379.
32 G. Subramanian, N. Mathew and J. Leiding, *J. Chem. Phys.*, 2015, **143**, 134109.
33 S. K. Jha, K. Brown, G. Todde and G. Subramanian, *J. Chem. Phys.*, 2016, **145**, 074307.
34 B. Chen, R. Hoffmann and R. Cammi, *Angew. Chem., Int. Ed.*, 2017, **56**, 11126–11142.
35 K. Wolinski and J. Baker, *Mol. Phys.*, 2009, **107**, 2403–2417.
36 G. Henkelman, B. P. Uberuaga and H. Jonsson, *J. Chem. Phys.*, 2000, **113**, 9901–9904.
37 G. Henkelman and H. Jónsson, *J. Chem. Phys.*, 2000, **113**, 9978–9985.
38 G. Henkelman, G. Jóhannesson and H. Jónsson, in *Theoretical Methods in Condensed Phase Chemistry*, ed. S. D. Schwartz, Springer Netherlands, Dordrecht, 2002, pp. 269–302.
39 M. J. Frisch, G. W. Trucks, H. B. Schlegel, G. E. Scuseria, M. A. Robb, J. R. Cheeseman, G. Scalmani, V. Barone, G. A. Petersson, H. Nakatsuji, X. Li, M. Caricato, A. V. Marenich, J. Bloino, B. G. Janesko, R. Gomperts, B. Mennucci, H. P. Hratchian, J. V. Ortiz, A. F. Izmaylov, J. L. Sonnenberg, D. Williams-Young, F. Ding, F. Lipparini, F. Egidi, J. Goings, B. Peng, A. Petrone, T. Henderson, D. Ranasinghe, V. G. Zakrzewski, J. Gao, N. Rega, G. Zheng, W. Liang, M. Hada, M. Ehara, K. Toyota, R. Fukuda, J. Hasegawa, M. Ishida, T. Nakajima, Y. Honda, O. Kitao, H. Nakai, T. Vreven, K. Throssell, J. A. Montgomery Jr., J. E. Peralta, F. Ogliaro, M. J. Bearpark, J. J. Heyd, E. N. Brothers, K. N. Kudin, V. N. Staroverov, T. A. Keith, R. Kobayashi, J. Normand, K. Raghavachari, A. P. Rendell, J. C. Burant, S. S. Iyengar, J. Tomasi, M. Cossi, J. M. Millam, M. Klene, C. Adamo, R. Cammi, J. W. Ochterski, R. L. Martin, K. Morokuma, O. Farkas, J. B. Foresman and D. J. Fox, *Gausian 16, Revision C.01*, Gaussian, Wallingford, CT, 2016.
40 D. Sheppard and G. Henkelman, *J. Comput. Chem.*, 2011, **32**, 1769–1771.
41 H. Spikes and W. Tysoe, *Tribol. Lett.*, 2015, **59**, 1–14.
42 S. M. Avdoshenko and D. E. Makarov, *J. Phys. Chem. B*, 2016, **120**, 1537–1545.
43 W. Quapp and J. M. Bofill, *Int. J. Quantum Chem.*, 2018, **118**, e25522.
44 W. Quapp, J. M. Bofill and J. Ribas-Ariño, *J. Phys. Chem. A*, 2017, **121**, 2820–2838.
45 J. M. Bofill, J. Ribas-Ariño, S. P. García and W. Quapp, *J. Chem. Phys.*, 2017, **147**, 152710.
46 R. Rana, G. Djuidje Kenmoe, F. Sidoroff, R. Bavisotto, N. Hopper and W. T. Tysoe, *J. Phys. Chem. C*, 2022, **126**, 11585–11593.
47 R. Rana, N. Hopper, F. Sidoroff and W. T. Tysoe, *Chem. Sci.*, 2022, **13**, 12651–12658.
48 W. Tysoe, *Tribol. Lett.*, 2017, **65**, 48.
49 K. L. Johnson, *Contact mechanics*, Cambridge University Press, 1985.
50 H. Adams, B. P. Miller, P. V. Kotvis, O. J. Furlong, A. Martini and W. T. Tysoe, *Tribol. Lett.*, 2016, **62**, 1–9.
51 H. Adams, B. P. Miller, O. J. Furlong, M. Fantauzzi, G. Navarra, A. Rossi, Y. Xu, P. V. Kotvis and W. T. Tysoe, *ACS Appl. Mater. Interfaces*, 2017, **9**, 26531–26538.
52 O. J. Furlong, B. P. Miller, P. Kotvis and W. T. Tysoe, *ACS Appl. Mater. Interfaces*, 2011, **3**, 795–800.
53 O. J. Furlong, B. P. Miller and W. T. Tysoe, *Tribol. Lett.*, 2011, **41**, 257–261.
54 B. Miller, O. Furlong and W. Tysoe, *Tribol. Lett.*, 2013, **49**, 39–46.
55 T. Thuening, J. Walker, H. Adams, O. Furlong and W. T. Tysoe, *Surf. Sci.*, 2016, **648**, 236–241.
56 H. L. Adams, M. T. Garvey, U. S. Ramasamy, Z. Ye, A. Martini and W. T. Tysoe, *J. Phys. Chem. C*, 2015, **119**, 7115–7123.
57 O. J. Furlong, B. P. Miller, Z. Li, J. Walker, L. Burkholder and W. T. Tysoe, *Langmuir*, 2010, **26**, 16375–16380.
58 M. Müser, *Phys. Rev. B: Condens. Matter Mater. Phys.*, 2011, **84**, 125419.
59 E. Gnecco, R. Roth and A. Baratoff, *Phys. Rev. B: Condens. Matter Mater. Phys.*, 2012, **86**, 035443.
60 S. J. Manzi, S. E. Carrera, O. J. Furlong, G. D. Kenmoe and W. T. Tysoe, *Tribol. Lett.*, 2021, **69**, 147.
61 G. Kresse and D. Joubert, *Phys. Rev. B: Condens. Matter Mater. Phys.*, 1999, **59**, 1758–1775.

 This journal is © the Owner Societies 2023

Published on 31 May 2023. Downloaded by University of Wisconsin-Milwaukee Libraries on 8/7/2023 6:46:01 PM.

62 P. E. Blöchl, *Phys. Rev. B: Condens. Matter Mater. Phys.*, 1994, **50**, 17953–17979.
63 G. Kresse and J. Hafner, *Phys. Rev. B: Condens. Matter Mater. Phys.*, 1993, **47**, 558–561.
64 G. Kresse and J. Furthmüller, *Phys. Rev. B: Condens. Matter Mater. Phys.*, 1996, **54**, 11169–11186.
65 G. Kresse and J. Furthmüller, *Comput. Mater. Sci.*, 1996, **6**, 15–50.
66 J. P. Perdew, K. Burke and M. Ernzerhof, *Phys. Rev. Lett.*, 1996, **77**, 3865.
67 H. J. Monkhorst and J. D. Pack, *Phys. Rev. B: Condens. Matter Mater. Phys.*, 1976, **13**, 5188–5192.
68 S. Grimme, J. Antony, S. Ehrlich and H. Krieg, *J. Chem. Phys.*, 2010, **132**, 154104.
69 M. Wühn, J. Weckesser and C. Wöll, *Langmuir*, 2001, **17**, 7605–7612.
70 G. Bell, *Science*, 1978, **200**, 618–627.
71 S. S. M. Konda, J. N. Brantley, C. W. Bielawski and D. E. Makarov, *J. Chem. Phys.*, 2011, **135**, 164103.
72 A. Bailey and N. J. Mosey, *J. Chem. Phys.*, 2012, **136**, 044102.
73 X. Chen, K. Kawai, H. Zhang, K. Fukuzawa, N. Koga, S. Itoh and N. Azuma, *J. Phys. Chem. C*, 2020, **124**, 22496–22505.
74 A. E. Stearn and H. Eyring, *Chem. Rev.*, 1941, **29**, 509–523.
75 R. Rana, R. Bavisotto, N. Hopper and W. T. Tysoe, *Tribol. Lett.*, 2021, **69**, 32.